2021

Empirical Indicated Loss Analysis of a Semi-hermetic Light-Commercial Spool Compressor

Seth Yarborough
Oklahoma State University, Seth.yarborough@okstate.edu

Craig R. Bradshaw
Oklahoma State University

Joe Orosz
Torad Engineering LLC

Greg Kemp
Torad Engineering LLC

Empirical Indicated Loss Analysis of a Semi-hermetic Light-Commercial Spool Compressor

Seth YARBOROUGH[1], Craig R. BRADSHAW[1*], Joe OROSZ[2], Greg KEMP[2]

[1]Center for Integrated Building Systems, Oklahoma State University, Stillwater, OK, USA, (405)744-5246
craig.bradshaw@okstate.edu

[2]Torad Engineering
Cumming, GA, USA, (678)366-3399
greg.kemp@toradengineering.com, joe.orosz@toradengineering.com

* Corresponding Author

ABSTRACT

An analysis of the indicated losses is presented for a semi-hermetic, light-commercial, prototype, spool compressor. The spool compressor prototype was instrumented with five high-speed pressure sensors, three in the process chamber, one in the discharge valve plenum, and one in the motor cavity. These sensors were triggered with a proximity sensor actuated by means of a custom rotary fixture attached to the compressor motor shaft. This coupling of rotational position and pressure measurements allowed for the development of an indicator (pressure v. volume) diagram for the compression process. Additionally, the added sensor in the discharge valve plenum allowed for a de-coupling of discharge valve losses and flow losses within the discharge plenum itself. The sensor in the motor cavity allowed for an analysis of the flow losses leaving the compressor shell. The compressor was tested at five motor speeds (1100, 1300, 1500, 1700 rpm and line voltage) at saturated condensing (SDT) and evaporating (SST) temperatures ranging from 37.8 – 48.9 °C (90 – 130 °F) and -3.8 – 15.6 °C(30 -60 °F), respectively at a fixed suction superheat of 11.1 K (20 °R) . Quantitative analysis shows that the suction and compression losses for this prototype compressor are relatively small compared with the discharge/valve losses. The total losses during the discharge process are generated by pressure drop and backflow through the discharge valve ports as well as when gas flows from the discharge plenum across the motor through the compressor body. It was found that a 5-6% improvement in compressor efficiency can be accomplished by redesigning the discharge plenum and motor cavity to reduce over pressurization. Further investigation into the valve dynamics need to be performed to improve the 11-12% loss in the valves. The valve losses were found to be sensitive to operating speed and SDT with maximum variations of 5% and 3%, respectively.

1. INTRODUCTION

Compressors in HVAC&R applications represent roughly 5% of total primary energy utilization[1] in the US. Therefore, to ensure maximum efficiency of new HVAC&R systems it is critical to evaluate and analyze new HVAC&R equipment, especially compressors. Novel compressors are especially critical to evaluate in great detail to ensure

[1] According to the US Energy Information Administration (EIA) , and the US Department of Energy (DOE) building data book , the consumption of electrical energy HVAC&R systems in the residential, commercial sectors corresponds to 22%, and 18%, of all primary energy annually in the US, roughly 40% in total. Compressors are estimated to account for roughly 60% of that energy consumed in cooling and refrigeration systems (Westphalen & Koszalinski, 2001). Resulting in an estimated 5% of the totally primary energy annually in the US.

adoption of new technology that creates a meaningful increase in system efficiency. Various methods over time have been used to evaluate the performance of compressors. The isentropic and volumetric efficiencies among other parameters are often used to evaluate bulk compressor performance. While those parameters can be useful for macro-analysis of compressor performance there is often a need for a more detailed breakdown of losses within a compressor.

1.1 Spool compressor background and motivation.

The rotating spool compressor is a novel rotary compressor mechanism most similar to the sliding vane compressor. Primary differences are described by Kemp *et al.* (2008) who first introduced the compressor applied to air-conditioning and refrigeration. Since its introduction, the spool compressor has undergone a large development effort including several prototype generations to represent air-conditioning applications from residential split-systems to commercial chiller products. Each prototype platform has presented additional insight into the unique attributes of this compressor and the best application of the device. This was accomplished by leveraging each prototype platform to further explore the spool compressor attributes by studying specific phenomenon/sub-systems during development.

The prototype spool compressor development progression through various application, displacements, and refrigerants has been investigated and summarized effectively in Bradshaw *et al.* (2018). The comprehensive model development and mechanism design improvements led to the 7th generation 40-ton, R134a spool compressor presented in Orosz *et al.* (2016)

Bradshaw *et al.* (2018) explored the potential for efficiency improvement by performing an indicated loss analysis on the 7th generation of prototype spool compressor, a 40-ton R134a prototype machine. The results of this study indicated the discharge plenum and valves had the largest room for improvement. A redesign of the discharge plenum was recommended for a potential 4-5% improvement in efficiency. The success of an indicated loss analysis on the 7th generation spool compressor prompted interest in exploring the potential improvement of the 8th and current generation of the prototype spool compressor, shown in Figure 1. The 8th generation of this compressor is a 30-ton R134a machine designed for air-conditioning applications and the first semi-hermetic embodiment of the mechanism. This study will present the experimental methodology, data analysis techniques, and indicated loss analysis results and suggest changes to the 8th generation prototype to maximize its efficiency.

2. Experimental Methodology

To generate an indicated loss analysis it is first necessary to measure dynamic pressure and compressor shaft position, which can be analyzed into the relevant losses. This section will focus on the collection and reduction of that data and generation of an indicator diagram. The general method to create an indicator diagram is to simultaneously measure both instantaneous chamber pressure and volume of a positive displacement compressor. The commonly used method to accomplish these measurements are often executed by mounting multiple pressure transducers into the compression chamber and measuring rotation angle of the shaft with a rotary encoder. Rotation angle is then used to calculate the volume of the compression chamber allowing for the indicator diagram to be created. Rigola *et al.* (2002) and Huang *et al. (2018)* used similar methods to produce indicated diagrams of reciprocation compressors. This is a process that follows closely with the work presented in Bradshaw *et al.* (2018) and this work continues from that effort.

The indicated loss analysis of the 8th generation spool compressor will follow similar methodology and the following section describes the installation and setup of the experiment to collect the data that creates an indicated loss analysis on the 8th generation spool compressor. This includes the sensor selection, placement, and calibration as well as an uncertainty analysis and the final test matrix of operating conditions that are collected and analyzed.

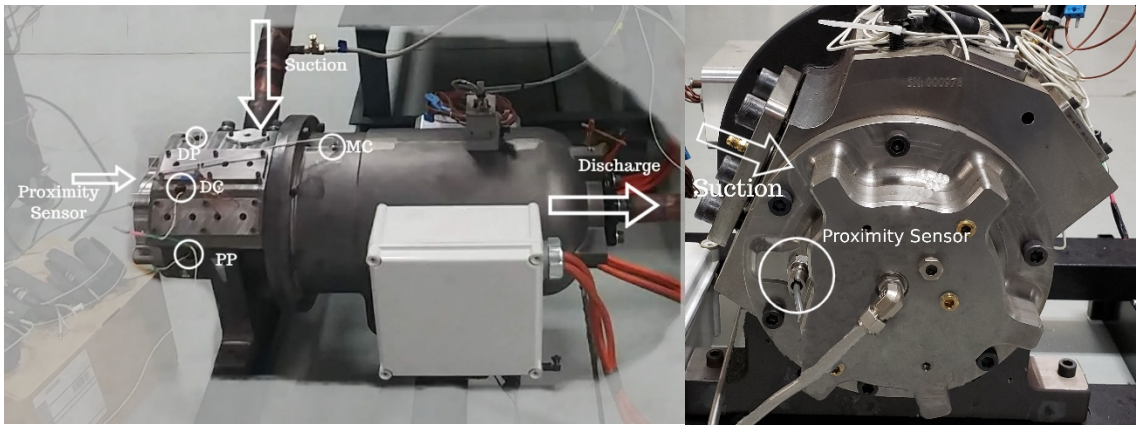

Figure 1: 8th generation, R134a, 30-ton, semi-hermetic, spool compressor prototype with high-speed pressure sensors installed showing motor cavity (MC) sensor, compression chamber (PP) sensor, discharge (DP) and discharge plenum (DC) (left) and the axial view showing the proximity sensor location. (right)

2.1 Sensor selection, location, calibration, and procedure

A 30-ton, semi-hermetic, prototype spool compressor is fitted with three Meggitt 8530B-500 high-speed pressure sensors at locations which will allow for easy installation of the sensors and for most of the process pressures to be measured at all rotor angles, called SP, PP, and DP, respectively. Additionally, two additional sensors were placed downstream of the discharge valve assemblies but upstream of the discharge manifold plumbing connection of the test stand, called DC and MC, respectively. Figure 1 shows the physical locations of these sensors relative to the suction and discharge of the compressor and the axial view of the physical location of the proximity sensor relative to the suction of the compressor. The angular locations of the three sensors in the process section are shown in Figure 2, which is an axial view schematic of the compressor cylinder with the sensor angles relative to Top-Dead-Center (TDC). The only regions which cannot be measured are near the TDC area of the compression process on both the suction and discharge side of the compressor. The volume in this region is insignificant when compared to the other volumes it is assumed that any losses or phenomenon that is unable to be measured is also small, therefore that loss in considered negligible.

The piezoresistive pressure transducers used in this analysis are susceptible to a change in the zero measured output as a result of electrical installation and mechanical installation (*i.e.* applied torque and wire strain). To mitigate the influence of error due to mechanical installation each of the five sensors was carefully installed with the recommended 1.69 N-m of torque and the strain on the sensors were minimized. To reduce influence as a result of electrical installation each sensor was electrically insulated at each of the connection points and were wired to ground at the signal conditioner. Each sensor was also calibrated in-place using dry nitrogen and a pressure reference measured using a Druck [DPI 612] with an accuracy of .0086 (0.125) bar (psia). The calibration was additionally repeated at the end of each set of tests to ensure no significant changes to the calibration occurred.

To measure shaft speed and position an inductive proximity sensor (Sensor Solutions S50FW-18ADSO-ODSB5) is used. The proximity sensor is arranged such that the sensor triggered when the vane of the compressor was at compressor Top Dead Center (TDC). This was used as a datum, or index, and all angles were measured in reference to this location. From the trigger, time is measured using the Data Acquisition Equipment (DAQ) and the shaft speed is assumed to be constant within one rotation. Using the measured time and the aforementioned assumption regarding speed allowed for an inference of the shaft position at any instant in the rotation.

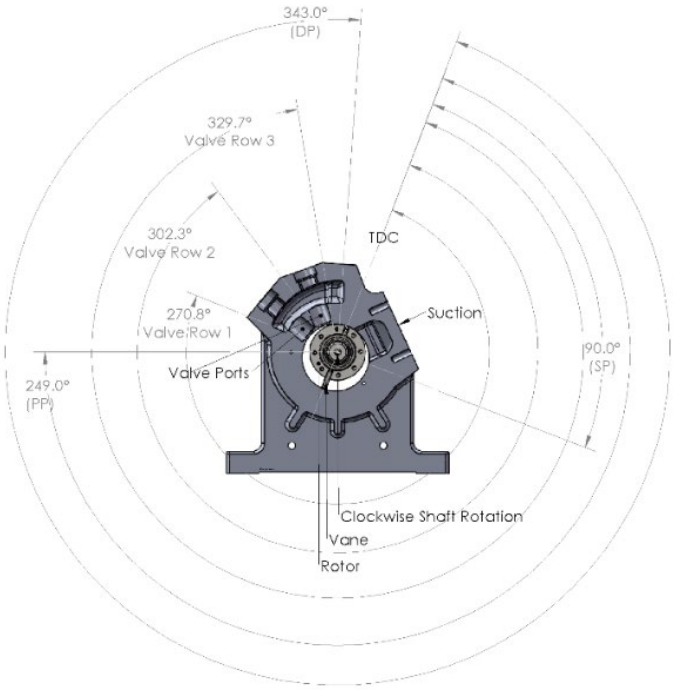

Figure 2: Axial view of compressor cylinder block highlighting the angular location of in-pocket sensors and valve location relative to vertical and the compressor top-dead-center (TDC).

2.2. Experimental procedure and test conditions

The compressor is first operated until it reaches steady-state conditions at a prescribed operating condition using the hot-gas bypass load stand environment described in Orosz *et al.* (2016). This load stand environment includes bulk pressure, temperature, and refrigerant mass flow rates as well as a means to control the conditions at steady-state. The pressure sensors are sampled at 70,000 samples per second (Hz), triggered using the inductive proximity sensor to start sampling at TDC, and sampled for a length of time that ensures at minimum of one complete rotation of the shaft for each test condition. This process was repeated 20 times per operating condition and these samples were averaged into a single sample which reflects the behavior at the current condition.

The prototype compressor was operated using refrigerant R134a at five shaft speeds, various Saturated Discharge Temperatures (SDT) and Saturated Suction Temperatures (SST) at a fixed compressor inlet superheat of 20 °R for a total of 36 data points. The final test matrix collected for this study is presented in Table 1. The limited SST range for certain speeds and SDT are constrained by the limits of the test environment. Test condition 8, bolded and underlined in Table 1, is used as the illustrative example, throughout this work as it represents the typical behavior of the compressor. The final pressures as a function of crank angle are presented in Figure 3 for Test condition 8. This figure also highlights the angular location of the different rows of valves in this compressor prototype, for reference.

3. DATA REDUCTION AND ANALYSIS

This section will present the procedures used to reduce the collected data, estimate the uncertainty associated with the calculated losses and calculate the suction, compression, and discharge indicated losses within the compressor. Additionally, two external indicated losses, the plenum and motor cavity, are also estimated as shown in this section.

3.1 Data reduction and Uncertainty

The uncertainty of the loss measurements is represented as a total relative uncertainty of the boundary work, as shown in the section below, this includes contributions from the high-speed pressure measurements and the volume calculation. The total uncertainty of the pressure measurement is calculated as a quadrature addition of the random

and systematic uncertainty. The systematic uncertainty of the pressure sensors is 0.172 (2.5) bar (psi) as verified by calibration and is assumed to be fixed. The random uncertainty in the pressure measurement is calculated using the 20 sample points taken per operating condition and calculated throughout the rotation of the shaft. The calculated total uncertainty of the pressure measurement ranged from 0.172 bar to 0.405 bar depending on the sensor and operating condition. The largest uncertainty consistently came from the discharge pressure sensor (DP). Test condition 8, from Table 1, has a total uncertainty of the pressure ranging 0.172 bar to 0.177 bar having a relatively small random uncertainty.

Table 1: Final test matrix of 36 operating conditions (presented with various saturated suction and discharge temperatures, SST and SDT, respectively) with a fixed 11.1 K superheat and shaft speeds high-speed measurements.

Speed	SST	Test #	SDT	Speed	SST	Test #	SDT
rpm	°C	-	°C	rpm	°C	-	°C
1100	4.4	5	37.8	1300	4.4	6	37.8
		4	43.3			3	43.3
		11	48.9			10	48.9
		12	54.4			13	54.4
1500	4.4	7	37.8	**1700**	1.67	34	48.9
		2	43.3		**4.4**	**8**	**37.8**
		9	48.9			1	43.3
		14	54.4			16	48.9
LV	-1.1	17	37.8			15	54.4
		18	43.3			32	32.2
		19	48.9			31	35.0
		20	54.4			33	48.9
	4.4	30	37.8		7.22	35	48.9
		27	43.3		12.78	36	48.9
		26	48.9				
		21	54.4				
	10	29	37.8				
		28	43.3				
		25	48.9				
		22	54.4				
	16	24	48.9				
		23	54.4				

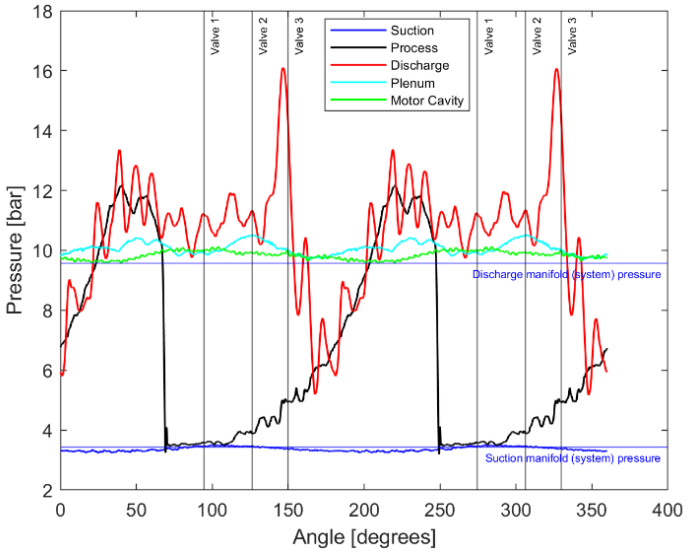

Figure 3: The five resulting pressure signals for test condition 8 from Table 1 as a function of compressor crank angle, highlighting the suction and discharge pressures measured at the load stand and overlaying the starting location of the discharge valve rows.

3.1.1 Uncertainty associated with fixed compressor speed assumption on the volume calculation

The inductive proximity sensor installed on the compressor will trigger once every rotation. To calculate the volume of the compressor at each instant requires an assumption that the rotational speed of the compressor remains constant throughout a single rotation. Large changes in shaft torque throughout the compression process necessitate that the shaft speed is not strictly uniform throughout a single rotation. To quantify the uncertainty of this assumption an analysis was performed using high-fidelity shaft position information collected from a similar spool compressor prototype, with data presented in Bradshaw *et al.* (2018). Bradshaw *et al.* (2018) collected data on an open-drive spool compressor prototype, with similar geometric characteristics and operating parameters as the compressor in this work, equipped with a 4096 steps/revolution rotary encoder that was also tested with R134a. Using the position data from the rotary encoder it is possible to estimate the variation in shaft speed over a rotation. For an operating condition similar to test condition 14, it was found that the shaft speed in the open-drive prototype varied by no more than 20 rpm.

The resulting differences in instantaneous volume are calculated using a fixed speed and the encoder speed was then estimated using the geometric model presented in Bradshaw and Groll (2013). It was found that the assumption of fixed speed would result in errors in volume averaging 0.67%. An additional assumption is then made that the open-drive and semi-hermetic mechanism operation is similar enough that the uncertainty in the both compressors volume calculations will be roughly the same.

The resulting total uncertainty from each of the two sources, volume and pressure, is used as an inputs to an uncertainty propagation analysis for the calculation of the boundary work as calculated following the procedure in equation 1. This analysis results in an error propagation of 0.85% for test condition 8 boundary work. This method follows ASME PTC 19.1 to combine the total uncertainty based on the respective loss expression described in the following sections.

3.2. Analysis of discharge losses

The discharge loss is a result of flow losses associated with the discharge port, valves, plenum, and flow into the motor cavity. Pressure drop associated with these areas result in a chamber pressure that is higher than the discharge manifold (system) pressure (p_{dis}) to overcome these losses. This loss is illustrated in Figure 4 and can be calculated using Equation 1 where the chamber pressure is equal to the discharge chamber (DP) during the discharge process, therefore the total discharge loss is calculated as,

$$L_{discharge} = \underbrace{-\int_{V_{min}}^{V_{dis,start}} p_{DP}\,dV}_{w_{BW,dis}} - \underbrace{\left(p_{dis}\left(V_{dis,start} - V_{min}\right)\right)}_{w_{ideal}}. \qquad (1)$$

where the boundary work is integrated between the minimum compression volume and the volume corresponding with the cylinder pressure exceeding the discharge manifold (system) pressure (p_{dis}). The location of the discharge sensor allowed for the entire discharge process to be captured by the discharge sensor.

The discharge loss can be further separated due to the additional pressure transducers in the discharge plenum and motor cavity. These two sensors allow for the discharge loss to be expanded into three separate losses, motor cavity loss, plenum loss, and valve loss. To separately capture the losses associated with the fluid leaving the discharge plenum the same technique is used using pressure data collected from the DC sensor. This assumes that the boundary work required to push fluid from the discharge plenum to the discharge manifold (system) pressure requires the same change in volume as the discharge process itself. Therefore, the total losses from discharge plenum can be evaluated as,

$$L_{dis,plenum} = \underbrace{-\int_{V_{min}}^{V_{dis,start}} p_{DC}\,dV}_{w_{BW,dis}} - \underbrace{\left(p_{dis}\left(V_{dis,start} - V_{min}\right)\right)}_{w_{ideal}}. \qquad (2)$$

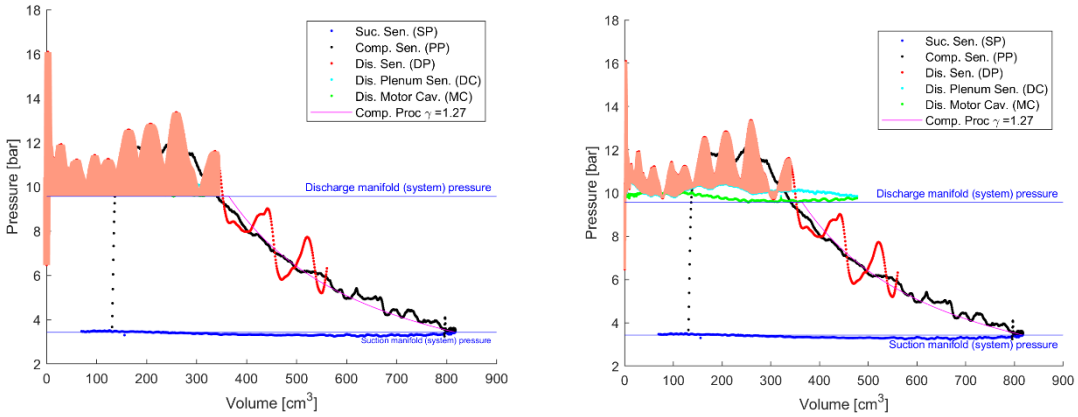

Figure 4: Indicator diagram of Test condition 8 highlighting the areas representing the total discharge loss (left) and the valve losses (right) as calculated by equations 1 and 3.

Following the same procedure at the discharge plenum the motor cavity losses are calculated using the MC sensor. Finally, taking the difference between the plenum losses and the total discharge losses the remainder is assumed to be dominated by the discharge valves/ports as shown by the shaded portion of Figure 4. Therefore, a derived loss is defined to capture this as,

$$L_{\text{valves}} = L_{\text{discharge}} - L_{\text{dis,plenum}}. \tag{3}$$

3.3 Analysis of compression losses

The compression process losses are associated with pressure during the closed compression process and calculated relative to an isentropic compression process. An isentropic compression process is modeled using a polytropic compression process where the polytropic exponent is assumed to be the ratio of specific heats of the refrigerant calculated at the various suction conditions of the compressor. The general expression to find the loss for the compression process is defined as,

$$L_{comp} = \quad -\int_{V_{max}}^{V_{dis,start}} (\, p_{PP} - p_{ideal}) dV, \tag{4}$$

where p_{ideal} is the isentropic compression process, $V_{dis,start}$ is the volume where the compression stops and discharge process begins, and $V_{\max}$ is the maximum volume of a single compression pocket.

3.4 Analysis of suction losses

Suction losses are associated with flow losses within the suction port as well as leakage that occurs during the suction process. These values are calculated using a similar procedure as the discharge process. The loss is therefore given as,

$$L_{comp} = \quad -\int_{V_{max}}^{V_{dis,start}} (\, p_{SP} - p_{suction}) dV. \tag{5}$$

4. RESULTS

This section presents results of the experimental campaign including a detailed breakdown of losses for the 30-ton spool compressor at test condition 8 and an analysis of the trends in the losses. Additionally, the losses are globally analyzed across the breath of conditions presented in the test matrix. Finally, a more detailed analysis of the compression losses is explored. The losses in this section are presented as percentage of total work measured from the compressor.

4.1 Loss breakdown at 40 °F SST, 100 °F SDT, and 1700 rpm (Test condition 8)

Figure 5 (left) shows the indicator diagram of operating condition Test condition 8 (left). Additionally, the suction manifold (system) pressure, discharge manifold (system) pressure and calculated isentropic work pressure is also overlaid on top of the data as a basis of comparison. The indicator diagram is also presented in this figure (right) with the three main loss areas shaded to reflect the areas used in the analysis presented in the previous section. The results of the analysis for Test condition 8 are collected in Table 2 and broken down by percentage loss associated with each loss mechanism as a percentage of total compressor work.

Table 2: Collection of losses for Test condition 8 presented as a percent of total work.

Test condition 8 Results					
Discharge	**Valves**	**Plenum**	**Motor Cavity**	**Suction**	**Compression**
%	**%**	**%**	**%**	**%**	**%**
18.04	12.16	3.21	2.67	1.78	.68

This table shows that the total discharge loss is by far the largest loss at 18.04% with a portion of that loss being associated with the plenum losses (3.21%) and the motor cavity losses (2.67%), leaving 112.16% of valve losses. Both the plenum and motor cavity losses are significant but neither one is as dominant as the discharge valve losses.

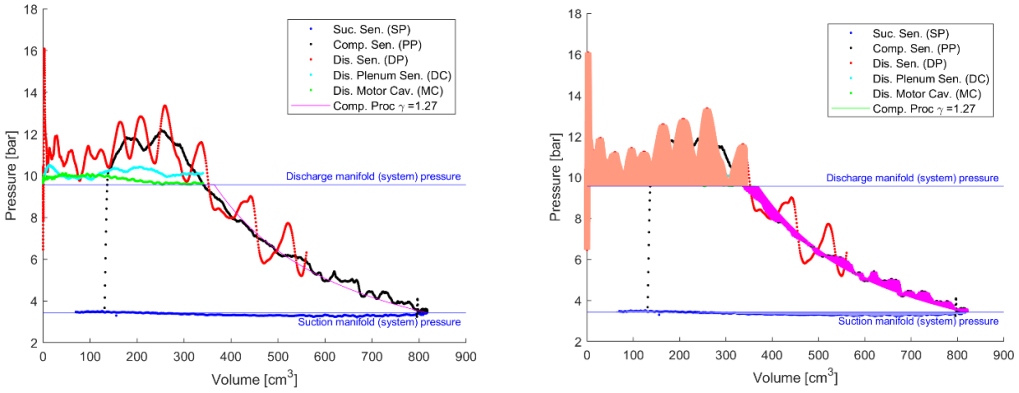

Figure 5: Indicator diagram of Test condition 8 with system suction and discharge pressures as well as the estimated isentropic compression process overlaid (left) and the loss areas shaded (right).

The suction loss (1.78 %) reflects the suction pressure measured blow the system pressure. Suction loss occurring in this manner is the typical expected loss that occurs at the suction port. The spool compressor tested doesn't have suction valves therefore this loss likely occurs as a result of pressure drop in the suction port.

The compression loss is relatively small despite not qualitatively matching the ideal compression process as shown in Figure 5. The measured process is closer to isothermal than the isentropic. Therefore, the specific work required is reduced and this results in a 'negative' loss for the portion of the process that approaches the start of the discharge process. This overcomes some of the additional work required to overcome the portion of the process just at the beginning of the compression process. Overall, the analysis from Test condition 8 suggested that the discharge plenum, motor cavity, and valve losses were the largest in the compressor and should be further explored.

4.2 Discharge plenum and valve losses

This section will expand on the single operating condition analysis by presenting the suction, compression, discharge, discharge plenum, motor cavity, and valve losses with various operating conditions with an emphasis of the three discharge-related losses.

Figure 6 presents the losses for the suction, compression, and discharge (left) and the plenum, motor cavity, and discharge (right) for speeds ranging from 1100 rpm to line voltage (approx. 1750 rpm) compressor shaft speeds at all the SST and SDT reported in Table 1. The suction, compression, motor cavity and plenum losses for all the speeds and operating conditions appear to show unremarkable trends. Figure 6 highlights that these four losses present with minimal trends with shaft speed. A separately analysis was also explored with SST and SDT and a trend wasn't discovered. The analysis does show a persistent loss of roughly 2-4% for suction, 0-1% for compression, 3-5% for plenum and 1-3% for the motor cavity. The addition of the motor cavity sensor has allowed for this distinction between the flow losses in the plenum and the motor cavity.

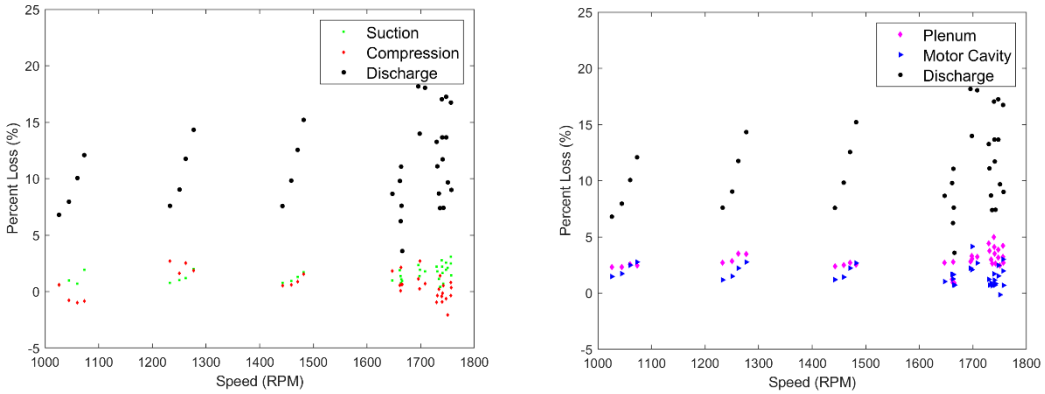

Figure 6: Indicated discharge plenum, motor cavity and valve losses shown for various speeds (right) and Indicated suction, discharge, and compression losses for various speeds (left). The marker size includes the experimental loss uncertainty.

In contrast, the valve losses show some significant trends as presented in Figure 7. The shaft speed and SDT correlate strongly with the valve loss. The valve loss increases by as much as 5% with speed while the loss decreases by as much as 3% at higher SDT conditions.

It is hypothesized that these losses are associated with either the discharge valves or the valve port/port placement. The valves are generally still not well understood. The results suggest that a significant performance improvement is possible with further optimization of the discharge process, most notably the valve performance..

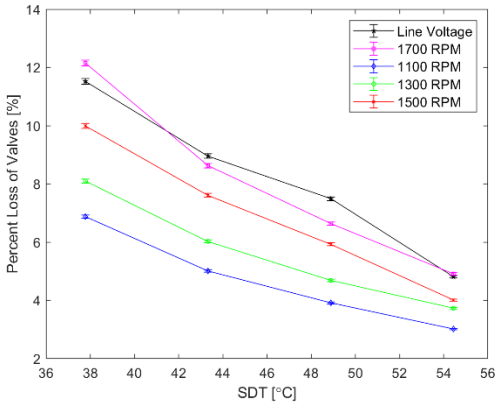

Figure 7: Percent Loss of discharge valves v. SDT at a constant 4.4 C (40F) SST for various speeds with error bars.

5. CONCLUSIONS

This paper presents an indicated loss analysis for the 8th generation 30-ton prototype spool compressor. The losses were collected using high-speed pressure measurements from five locations within the compressor and synchronized

with a proximity sensor as the trigger mechanism. The results suggest that the largest simple opportunity for improvement in this prototype is a re-design of the discharge plenum. This re-design has the potential to result in 3-4% improvement in the overall compressor efficiency. Additionally, a redesign of the motor cavity could add an additional potential improvement of 2-3%.

The valve losses presented an increasing trend with increasing speed and decreasing SDT. The valve improvements presented are the largest potential improvement with losses ranging from 9-18% depending on speed and operating condition. The valve losses presented as somewhat independent of suction conditions but relatively sensitive to discharge condition. The indicated losses of the valves indicate that more study of the dynamics of the valves is necessary to ensure the losses are mitigated across the entire operating range.

NOMENCLATURE

L	indicated loss	(Btu, kJ)
p	pressure	(psia, kPa)
V	volume	(in^3, m^3)
w	specific work	(Btu, kJ)

Subscript

BW	boundary work
comp	compression process
dis, plenum	discharge plenum portion of discharge
dis, start	start of discharge process
discharge	total discharge process
DC	discharge cover/discharge plenum
DP	discharge pocket
MC	motor cavity
ideal	ideal process
PP	process/compression pocket
suc, suction	suction process
SP	suction pocket
valves	valve portion of discharge

REFERENCES

ASME PTC 19.1-2018, Test uncertainty, ASME. 2018.

Bradshaw, C. Spool compressor tip seal design considerations. In 8th International Conference on Compressors and their Systems (2013), p. 341.

Bradshaw, C. R., and Groll, E. A. A comprehensive model of a novel rotating spool compressor. International Journal of Refrigeration 36, 7 (2013), 1974 – 1981. New Developments in Compressor Technology.

Bradshaw, C. R., Kemp, G., Orosz, J., and Groll, E. A. Development of a loss pareto for a rotating spool compressor using high-speed pressure measurements and friction analysis. Applied Thermal Engineering 99 (2016), 392–401.

Kemp, G. T., Garrett, N., and Groll, E. A. Novel rotary spool compressor design and preliminary prototype performance. In International Compressor Engineering Conference at Purdue University (2008), no. 1328.

Orosz, J., Bradshaw, C., Kemp, G., and Groll, E. Updated performance and operating characteristics of a novel rotating spool compressor. In International Compressor Engineering Conference (2016), no. 1377.

Rigola J., Pérez-Segarra C. D., Raush G., Oliva A., Escribà M., Jover J., and Escanes F. (2002). Experimental Studies of Hermetic Reciprocating Compressors with Special Emphasis On PV Diagram. International Compressor Engineering Conference, Paper 1506. https://docs.lib.purdue.edu/icec/1966

US Energy Information Administration (EIA) Electric Power Monthly, Table 5.1 (2011)

US Department of Energy (DOE) 2010 Buildings Energy Data Book, Sections 2.1.5 and 3.1.4 (2011)

Westphalen, D. and S. Koszalinski 2001. Energy Consumption Characteristics of Commercial Building HVAC Systems Volume I : Chillers, Refrigerant Compressors and Heating Systems.